Placenta xxx (xxxx) xxx

Contents lists available at ScienceDirect

Placenta

journal homepage: www.elsevier.com/locate/placenta

Exploring placental ultrastructure: A review of electron microscopy techniques and emerging methods for resolving 3D organelle architecture

Siddharth Acharya [a,b], Eric Hanssen [c,d], James C. Bouwer [e,f], John E. Schjenken [a,g], Kirsty G. Pringle [a,b], Roger Smith [a,h], Joshua J. Fisher [a,h,*]

[a] Reproductive and Family Health Program, Hunter Medical Research Institute, New Lambton Heights, NSW, Australia
[b] School of Biomedical Sciences and Pharmacy, College of Health, Medicine and Wellbeing, University of Newcastle, Callaghan, NSW, Australia
[c] Ian Holmes Imaging Centre and ARC Industrial Training Centre for Cryo-electron Microscopy of Membrane Proteins, The Bio21 Molecular Science and Biotechnology Institute, University of Melbourne, Parkville, VIC, Australia
[d] Department of Biochemistry and Pharmacology, University of Melbourne, Parkville, VIC, Australia
[e] Molecular Horizons and School of Chemistry and Molecular Bioscience, University of Wollongong, Wollongong, NSW, Australia
[f] ARC Industrial Transformation Training Centre for Cryo-electron Microscopy of Membrane Proteins, University of Wollongong, Wollongong, NSW, Australia
[g] School of Environmental and Life Sciences, College of Engineering, Science and Environment, University of Newcastle, Callaghan, NSW, Australia
[h] School of Medicine and Public Health, College of Health, Medicine and Wellbeing, University of Newcastle, Callaghan, NSW, Australia

ARTICLE INFO

Keywords:
Placenta
Organelles
Mitochondria
Volume electron microscopy
3D structure
Cryo-EM

ABSTRACT

Trophoblast cells line the surface of placental villi, facilitating the exchange of nutrients, gases, and wastes between the maternal and fetal circulations. The fusion of cytotrophoblast (CTB) cells into the surrounding multinucleated syncytiotrophoblast (STB), is accompanied by a shift in cellular ultrastructure (subcellular architecture). Mitochondria undergo a remarkable decrease in size and alteration in morphology following trophoblast differentiation, and have thus been the subject of investigations due to their crucial role in producing energy for placental development. Observing this shift in structure has relied on the use of electron microscopy, which has offered insights into underlying mitochondrial functions. Since the initial use of electron microscopy to study villous trophoblasts in the 1950s, novel techniques have emerged that have the capacity to interrogate placental ultrastructure with unprecedented resolution. This review discusses the evolution of electron microscopy techniques to study the placenta over the last 70 years. Moreover, we discuss emerging methods for resolving 3D organelle structure within the placenta, which offer more physiologically pertinent information and context for complex topologies. Further, we discuss advanced methods of cryo-electron tomography (cryo-ET) that present the placental field with an exciting opportunity to determine the complex relationship between mitochondrial architecture and protein structure in the human placenta. By specifically focusing on mitochondrial imaging, we showcase the capacity for volume electron microscopy and cryo-ET to reveal the role of organelle structure in placental development.

1. Introduction

Trophoblast cells line the surface of placental villi, facilitating placental implantation, maternal-fetal nutrient exchange, and steroidogenesis [1–3]. In order to fulfill these functions, trophoblasts rely upon cellular ultrastructure (subcellular architecture) [4]. Adjacent to the basement membrane, progenitor epithelial, proliferative cytotrophoblasts (CTB) fuse and differentiate into the outer, multinucleated syncytiotrophoblast (STB). Following differentiation, the ultrastructure is reorganised, and organelles undergo structural remodelling to meet altered cellular functions [4–7]. Since the initial use of electron microscopy to study villous trophoblasts in the 1950s, techniques have emerged that have the capacity to advance our understanding of placental ultrastructure, and contribute to a greater understanding of placental function.

Studying the ultrastructure of the placenta involves resolving subcellular features that are smaller than the wavelength of light (400–650 nm), which renders optical microscopy techniques ineffective. Given

This article is part of a special issue entitled: Advanced placental imaging published in Placenta.

* Corresponding author. Reproductive and Family Health Program, Hunter Medical Research Institute, New Lambton Heights, NSW, Australia.
E-mail address: Joshua.fisher@newcastle.edu.au (J.J. Fisher).

https://doi.org/10.1016/j.placenta.2026.01.009
Received 21 November 2025; Received in revised form 8 January 2026; Accepted 15 January 2026
Available online 16 January 2026

that the wavelength of an electron is up to 100,000 times smaller than the wavelength of light, electron microscopy instead applies a focused beam of electrons to resolve the cellular ultrastructure [8,9]. Electrons are emitted from an electron gun either via thermionic emission (by heating a tungsten filament) or field emission (by applying a strong electric field to a sharp tungsten tip) [10,11]. Subsequently, emitted electrons are accelerated and focused by electromagnetic condenser lenses and apertures, followed by an objective lens. Depending on how the electrons are focused to interact with the tissue, electron microscopy can be separated into two broad categories; transmission electron microscopy (TEM) and scanning electron microscopy (SEM).

In TEM, electrons are transmitted through a thin section of tissue (typically sectioned to ~100 nm via ultramicrotome) and may pass through unscattered, or undergo either elastic scattering (resulting in backscattered electrons) or inelastic scattering (where the energy is transferred to the atoms within the sample, producing secondary electrons) [12]. Transmitted and scattered electrons are collected to form the image, providing high-resolution information about the sample. In SEM, electrons are focused on the surface of the sample and either elastically scattered or inelastically scattered. Backscattered electrons provide information about sample composition as heavier elements scatter more strongly and therefore appear brighter, whereas secondary electrons provide information on sample surface topography [13]. In both TEM and SEM, the electron beam is operated in a vacuum to avoid the collision of electrons with air particles, therefore biological samples must be fixed, dehydrated, embedded in resin and sectioned, and then impregnated with heavy metals to increase contrast of biological features, and dehydrated prior to examination (Fig. 1A). While the standard application of TEM produces 2D images, a sample can be imaged at several tilt angles to produce a tomographic 3D reconstruction, albeit at a lower resolution compared to cryogenic electron tomography (cryo-ET) [14]. Using SEM, sections of a sample can be serially imaged through a collection of techniques known as 'volume electron microscopy' to resolve the 3D ultrastructure of the sample (Fig. 1B) [15].

Cryo-ET, a technique that has become more accessible over the last 10 years as a result of the simplification of automation and software, is capable of achieving near atomic-level resolution detail (<10 Å) of cellular ultrastructure, isolated organelles, or purified proteins (Fig. 1C) [16]. In contrast to standard TEM and SEM, which uses chemical fixation and dehydration thereby introducing preparation artifacts, cryo-ET derives its name from the use of cryogenic temperature during image acquisition, and the use of samples that are vitrified in amorphous ice [16]. Vitrification preserves the native molecular structure without the need to dehydrate the biological samples, allowing the retention of physiological structures. Imaging at cryogenic temperatures also limits beam-induced damage, permitting the collection of multiple micrographs at various tilt angles (typically ± 60°) that are used to perform tomographic reconstruction [17]. Moreover, while under cryogenic conditions, and before observation in a cryoTEM, samples may be thinned using a focused-ion-beam SEM (FIB-SEM), producing an ultrathin section that optimises the signal-to-noise and contrast ratios for the determination of protein structures in situ [18]. The advent of cryo-ET presents the placental research field with an exciting opportunity for observing trophoblast organelles with unprecedented resolution. Such insights will greatly improve our understanding of the links between organelle and protein structure and placental function.

This review will discuss the last 70 years of advances in electron microscopy and its application to study placental ultrastructure, with a particular focus on imaging mitochondria and other subcellular organelles. The focus on imaging and further understanding mitochondria, provides insights into the morphology shifts during trophoblast differentiation, while the methods discussed could be applied to all subcellular structures and organelles. Thus, we highlight the substantial potential to reveal subcellular processes that regulate differentiation and placental function that currently remain unknown. As such, we discuss emerging 3D electron microscopy techniques and address current limitations in the field related to the extraction of biological information from imaging data.

2. Early applications of electron microscopy to study villous trophoblasts

Trophoblast ultrastructure, particularly the morphology of organelles within progenitor CTB and the differentiated STB, has been the subject of investigation since the 1950s, following initial observations by *Wislocki & Dempsey* of the morphological variations between CTBs and the STB [19–21]. In a pioneering study by *Boyd & Hughes* in 1954, fixed placental villi sections were imaged by TEM, revealing that the STB has a darker cytoplasm and more irregular nuclei compared to the CTB (Fig. 2A) [22]. While these findings were significant in the placental field, they were limited by microscope technology of the time [22]. Modern TEMs supersede the early microscopes used by *Boyd & Hughes* in critical aspects that contribute to image quality, including the use of ultra-high vacuums, better image processing (such as aberration correction that prevents blurring and distortion), and improved microscope machining [23–25]. Additionally, the use of field emission guns instead of thermionic emission guns allowed for brighter and more coherent electron beams, thus improving spatial resolution and contrast [10]. Perhaps the most substantial improvement to the efficiency of electron microscopy, has been the implementation of digital cameras, which have replaced the glass and film photographic plates that were used by *Boyd & Hughes* in the 1950s [22]. Indeed, chemically developed electron micrographs offered exceptional resolution, constrained only by the size of the silver-halide grains, and could be enlarged 5–10 fold without pixelation, depending on the acquisition parameters [26–28]. Moreover, such analogue methods provided a wide range of contrast, with artifacts or irregularities from light distribution that could be corrected in a darkroom, a process that remains challenging with digital micrographs. Additionally, the resulting negatives and film provided a stable means of physical storage, capable of lasting up to hundreds of years without deterioration if stored under archival conditions, and far exceeding the lifespan of even modern hard disk and solid-state drives [29]. However, digital cameras have significantly increased the rate of data collection, enabled immediate on-the-fly image processing and analysis, permitted the correction of beam-induced motion, and improved reproducibility of image acquisition [30,31]. Regardless of the throughput limitations in the 1950s, the early studies revealed the distinct morphological diversity between undifferentiated CTBs and the differentiated STB [22].

In the late 1950s and 1960s, detailed TEM analyses of trophoblast ultrastructure and organelle distribution were published by *Dempsey*, *Wakitani*, *Boyd & Hamilton*, *Castellucci & Kaufmann*, and subsequently by *Jones & Fox* in 1991 (Fig. 2B) [4,5,32–35]. Over a decade after these studies, SEM performed by *Burton*, provided detailed topological information of microvilli covering the surface of the placental villi [36]. Amongst other findings and of particular relevance to this review, these studies were the first to show that STB mitochondria (Syncytio-Mitos) were much smaller and more electron-dense than CTB mitochondria (Cyto-Mitos) [4,5,32–35]. As of 2025, refined protocols have allowed observations of trophoblast ultrastructure in greater detail, revealing striking variation within the villi and accompanying cell lineages. Our own imaging supports previous observations of organelles in the STB by *Martin & Spicer* and *Jones & Fox*, including lipid droplets, vesicles, vacuoles, and an intricate microvillous membrane (unpublished observations, Fig. 2C) [4,37].

The development of staining methodologies has enabled improved visualisation of cellular ultrastructure by optimising the contrast of phospholipid membranes, nucleic acids, and the localisation of organelles. Perhaps the most notable use of advanced staining methods to study the STB was by *Martinez* et al., who used immunogold labelling to identify a higher abundance of steroidogenic cholesterol side-chain cleavage enzyme ($P450_{SCC}$) within mitochondria of the STB, compared to the CTB [38]. The application of immunolabelling has permitted unambiguous localisation of organelles, such as mitochondria, and has provided insights into their steroidogenic capacity in the placenta [38]. The continued optimisation of sample preparation techniques has significantly improved the attainable resolution, contrast, and clarity of

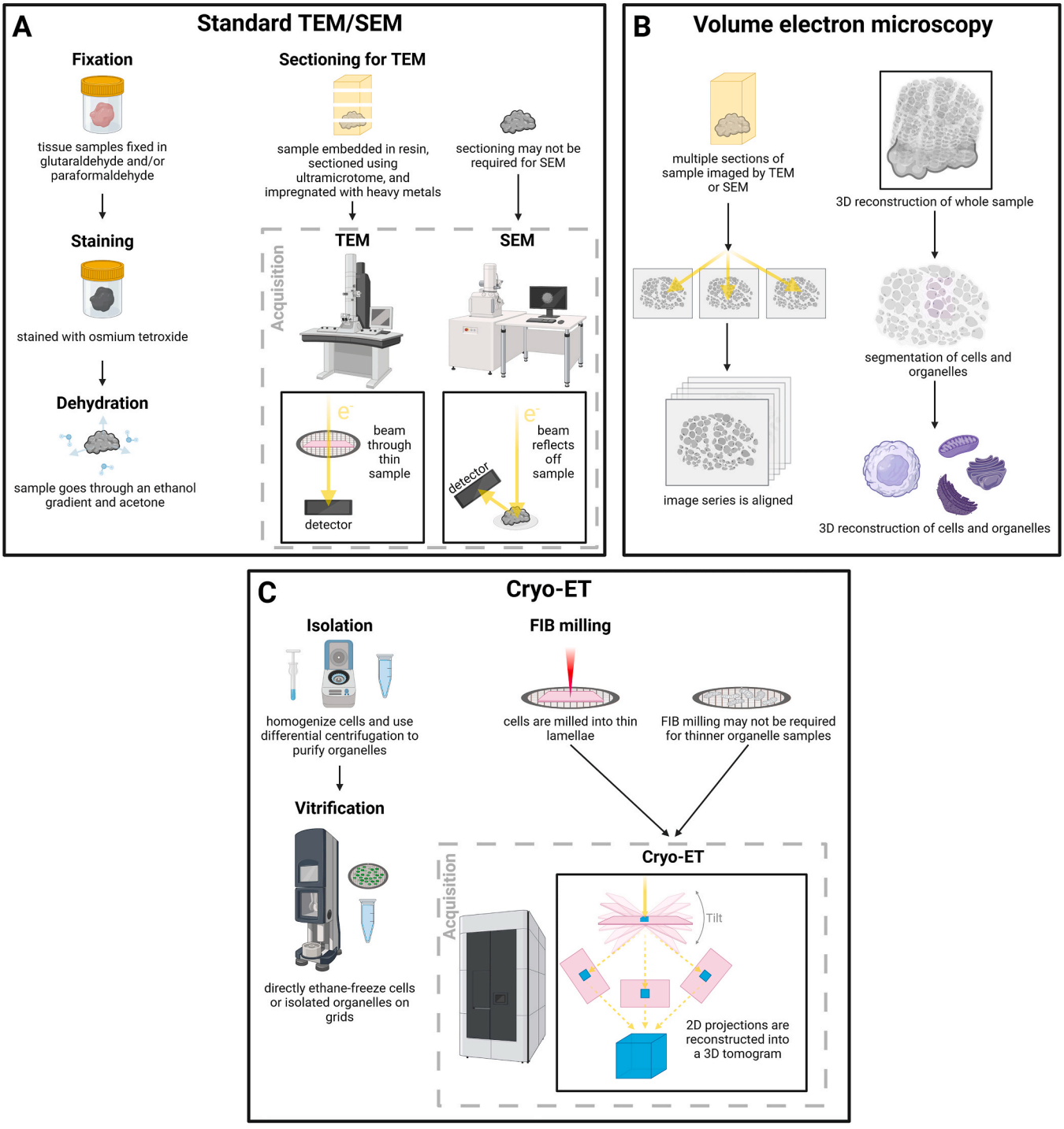

Fig. 1. An overview of electron microscopy. A) The process of preparing samples for standard transmission electron microscopy (TEM) and scanning electron microscopy (SEM), which involves fixing samples, dehydration and resin embedding, and staining the sections to improve contrast. Samples are typically embedded in resin and sectioned for TEM, or may be imaged directly for SEM. B) The process for collecting data for volume electron microscopy, which involves imaging multiple sections of a sample in succession. The series of micrographs are aligned to reconstruct the whole sample, or cells and organelles of interest may be segmented for 3D reconstructions of ultrastructure. C) The process of preparing samples for cryo-ET, which involves homogenising cells and using differential centrifugation to separate and purify organelles based on density. Enriched organelle populations are then be vitrified on grids. Whole cells may also be vitrified, but require focused-ion-beam (FIB) milling to prepare thin sections for cryo-ET. Samples are tilted within the microscope, and 2D projections at various tilt angles are reconstructed into a 3D tomogram.

organelles within the trophoblast bilayer. Current preparation techniques also include staining with potassium ferricyanide (further enhancing the contrast of mitochondria, endoplasmic reticulum, and Golgi) and thiocarbohydrazide (which improves osmium tetroxide deposition), in addition to osmium tetroxide, lead citrate, and uranyl acetate [39]. Collectively with improved imaging signal, contrast, and resolution, our ability to resolve the ultrastructure of the trophoblast bilayer, and specifically mitochondrial structure, has significantly improved since the seminal works of the 1950s.

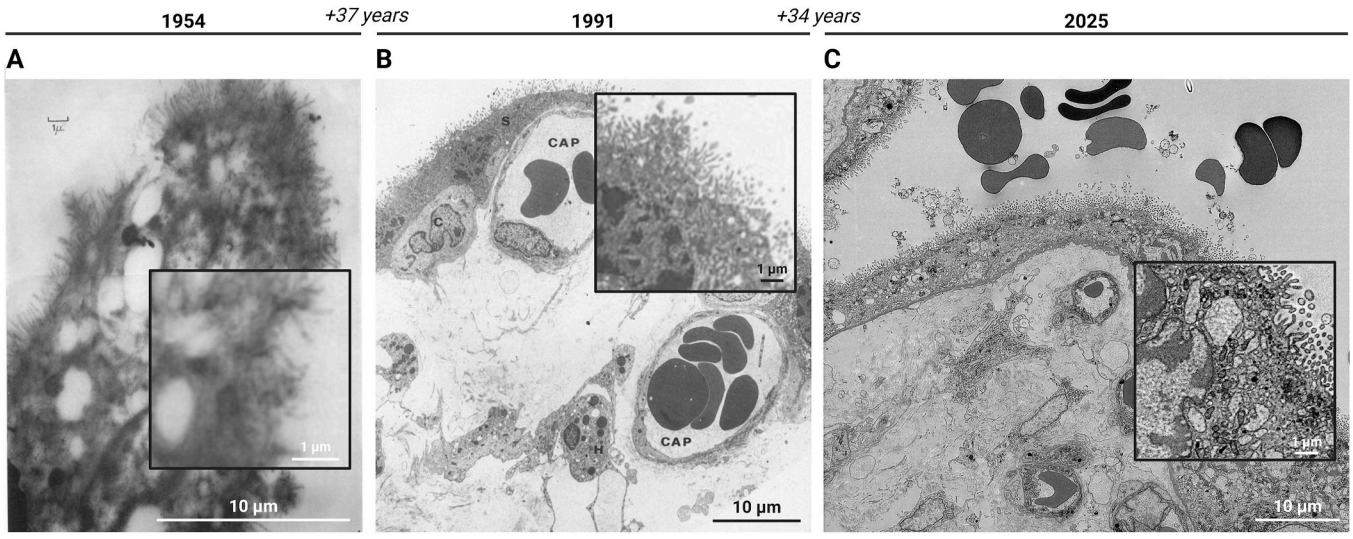

Fig. 2. 70 years of placental villi imaging. A) Transmission electron microscopy (TEM) of placental villi section performed in 1954 [22]. B) TEM of placental villi section performed in 1991 [4]. C) Healthy placental tissue was fixed, stained, dehydrated, and embedded in resin prior to ultramicrotome sectioning. In 2025, we performed backscatter scanning electron microscopy (SEM) using the Teneo VolumeScope (Thermo Fisher Scientific, USA), with a final pixel size of 16 nm. Scale bars represent 10 μm in the main images, or 1 μm in the magnified regions.

3. Techniques for resolving 3D organelle architecture

3.1. The implications of mitochondrial form on function

Following on from the observation that there is increased $P450_{SCC}$ in the STB, *Martinez* et al., proposed that STB mitochondria have an increased surface area to volume ratio for efficient cholesterol import and pregnenolone synthesis [38]. Through assessing both mitochondrial structure and steroidogenic function, it was suggested that vesicular-shaped cristae (folds of the inner mitochondrial membrane) were present in mitochondria of the STB for high steroidogenic capacity, supporting the work of *Terzakis* and *Tighe* et al. [38,40,41]. Until 2015, it was also believed and entrenched in dogma within the placental field, that the STB performed the majority of the metabolic roles of the placenta, compared to the CTB. *Kolahi* et al., challenged these ideas surrounding trophoblast bioenergetics, and showed that CTBs dominate placental metabolism and have higher respiratory rates than the STB [42]. *Kolahi* et al., also used fluorescence microscopy to show that CTB mitochondria were more elongated and formed tightly packed networks, while STB mitochondria were fragmented. These findings were supported by *Fisher* et al., who showed that isolated and enriched fractions of CTB mitochondria had a greater maximum respiratory capacity and produced more ATP compared to STB mitochondria [6]. However, in both instances, these observations were made using 2D imaging without the capacity to define complex 3D mitochondrial networks [42].

Since the early investigations of trophoblast ultrastructure, TEM and SEM of either placental tissue or isolated mitochondria, have both shown that CTB mitochondria are larger and more abundant with cristae, compared to STB mitochondria [4,6,38]. While these traditional imaging techniques have shown the diversity of mitochondrial populations in 2D cross sections, they provide limited information regarding the topologically complex nature of mitochondrial networks or physiologically pertinent metrics of surface area and volume [43]. In 2D, mitochondria appear as separated organelles with distinct outer membranes and morphologies depending on the intersecting plane of the image, be that horizontal, vertical, or transverse cross-sections. However, following a single placental mitochondrion in full throughout the depth of the cell, and producing a 3D reconstruction, reveals the extent of mitochondrial branching and topological complexity (Fig. 3A) [7,44]. Additionally, the specific orientation of each organelle can alter their apparent size in cross-sections, making quantitative and statistical analysis challenging [45]. This is particularly the case when observing placental mitochondria from the CTB and STB in 2D, which may appear rounded or circular if sectioned through the sagittal plane, but extend in the Z-axis to form elongated bodies (Fig. 3B–D) [45]. Moreover, through full reconstruction of all mitochondria within a cell, the interconnectedness between mitochondria becomes apparent [7]. Furthermore, inferring 3D topology from 2D imaging is challenging, since mitochondria undulate and follow sinuous paths around neighbouring organelles, including other mitochondria [7,45]. As such, ensuring that mitochondrial structure and morphology is appropriately characterised in the 3D space is essential for understanding the role of altered structure in mitochondrial pathology and disease, such as mitochondrial myopathies characterised by swollen mitochondrial phenotypes in 2D [46]. This structural abnormality of mitochondria extends to placental pathologies such as fetal growth restriction and preeclampsia, reviewed elsewhere by *Holland* et al. [47].

Given the essential role of mitochondrial networks in supporting bioenergetic and steroidogenic demands in the placenta, there exists a need to quantitatively assess 3D mitochondrial structure within the native tissue environment [6,7,38,42]. Therefore, volume electron microscopy is crucial for observing the consequences of mitochondrial fusion and fission [48,49].

3.2. From 2D to 3D: revealing mitochondrial network structure and gross morphology

Imaging intact mitochondrial networks requires the application of volume electron microscopy on whole placental tissue. Like TEM and SEM, samples are chemically fixed and stained with heavy metals (often at higher concentrations in volume electron microscopy to improve backscatter contrast) and then dehydrated using an ethanol and acetone gradient [39,50,51]. However, for volume electron microscopy, samples are typically embedded in larger resin blocks, using harder resin that withstands repeated sectioning and electron exposure, as opposed to single doses when imaging in 2D [39]. Three primary volume electron microscopy techniques include FIB-SEM tomography, serial block-face SEM (SBF-SEM), and array tomography, all of which use SEM for imaging. Each of these three techniques have their own advantages and limitations, summarised in Table 1. While FIB-SEM tomography typically affords the highest resolution compared to SBF-SEM and array tomography, large samples require lengthy acquisition times making this technique expensive to perform. SBF-SEM is capable of imaging

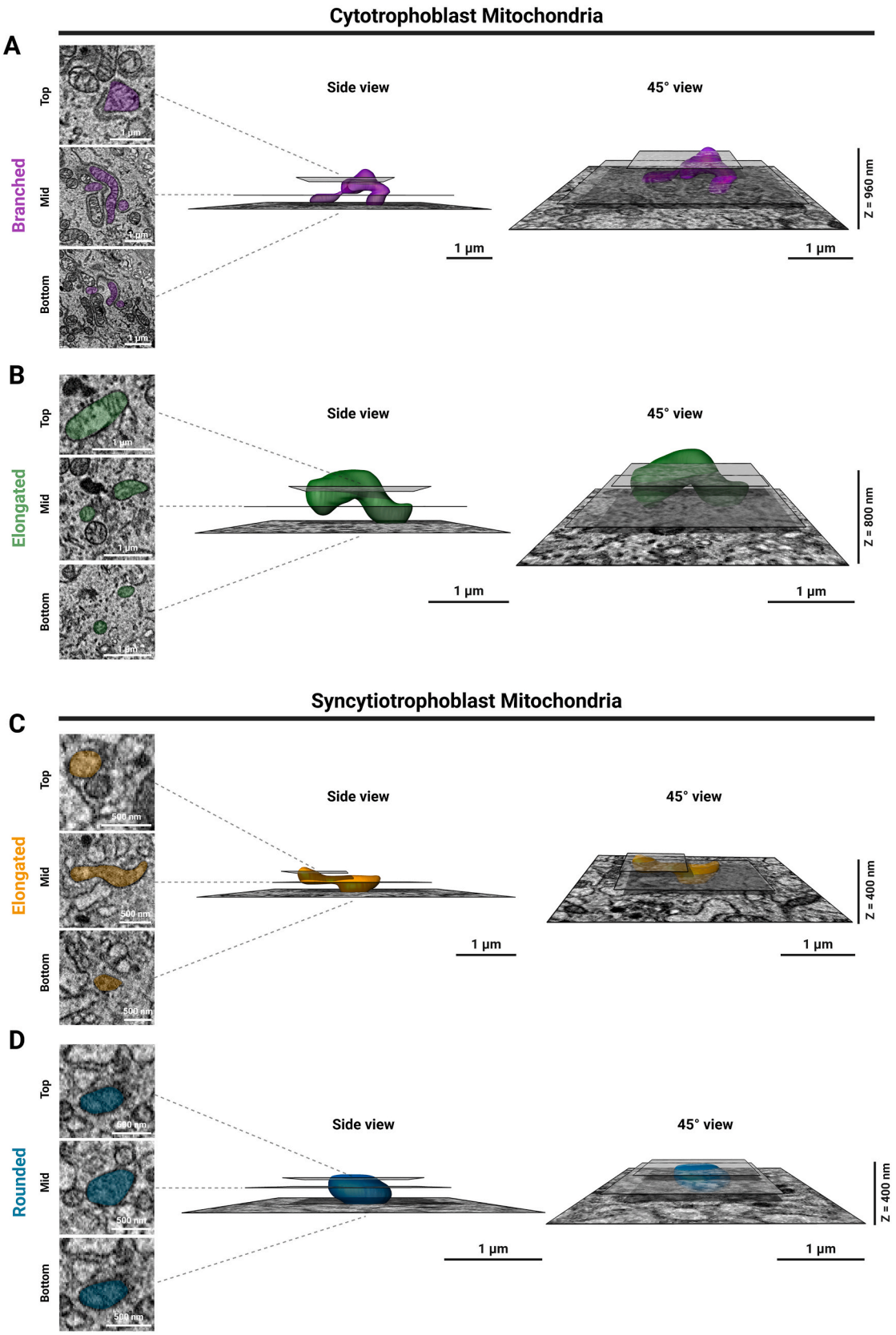

Fig. 3. Orientation of mitochondria in cross-sections reflects apparent size. Human placental tissue was fixed, stained, dehydrated, and embedded in resin. Samples were sectioned at a thickness of 80 nm by ultramicrotome, and sections were collected onto silicon wafers. Array tomography was performed, collecting micrographs of over 200 sections that were aligned, permitting segmentation and 3D reconstruction of Cyto- and Syncytio-Mitos. A) Branched Cyto-Mito (purple), B) Elongated Cyto-Mito (green), C) Elongated Syncytio-Mito (yellow), and D) Rounded Syncytio-Mito (blue) reconstructions shown with their corresponding micrographs obtained from the top, middle, and bottom of the Z-stack, with the total Z-depth shown for each reconstruction (nm). Scale bar represents 1 µm.

Table 1
Advantages and limitations of volume EM techniques.

	Advantages	Limitations	Best Suited For
FIB-SEM Tomography	High XYZ-resolution (~3–10 nm). Isotropic voxels (equal XY and Z). May be paired with correlative imaging.	Large non-conductive samples prone to charging. Long acquisition time (>24 h). Destructive, sample is lost. Limited to smaller sample volumes (~10 μm in XYZ). Prone to milling artifacts (curtaining).	Isotropic nanometre-resolution detail of individual cells and small organelles.
SBF-SEM	Moderate XY-resolution (~5–20 nm). Large sample volume (10–100 μm in XYZ). Highly automated.	Lower Z-resolution (~20–100 nm). Large non-conductive samples prone to charging. Destructive, sample is lost.	Nanometre-resolution detail of larger samples.
Array Tomography	High XY-resolution (~3–10 nm). Moderate Z-resolution (~30–70 nm). Less sample charging. Can stain individual sections with immunofluorescent antibodies for more optimised correlative imaging. Large samples can be imaged using tiled acquisition (100–1000 μm in XYZ). Non-destructive, sample is recovered. Incorporation of automated tape collecting ultramicrotome (ATUM) can improve the efficiency of section collection.	Technically challenging due to manual sectioning. Large volume data requires substantial computational resources. Potential loss of continuity in image series. Image artifacts from sectioning (compression).	Very large samples with the option of fluorescent labelling, correlative imaging, and reimaging sections.

larger sample volumes but results in a lower Z-resolution. Since both FIB-SEM and SBF-SEM requires the whole sample block to be subject to the electron beam, these techniques are subject to excessive charging, whereby excess electrons are absorbed by the sample and may become trapped [52]. When these electrons discharge, the microscope's electron detectors inaccurately interpret these signals, causing image artifacts, reduced contrast, or even sample damage [52]. Furthermore, sections imaged by FIB-SEM or SBF-SEM are lost in the process and cannot be recovered or re-imaged. In array tomography, samples are non-destructively imaged with high resolutions in both XY and Z, and sections may be stained with immunofluorescence labels, however the technique is challenging to perform, and images are prone to sectioning artifacts. Such challenges may be addressed by incorporating an automated tape collecting ultramicrotome (ATUM), which collects sections onto moving tape, and is more efficient for high-throughput large data collection and reduced section loss [53]. By using the volume electron microscopy technique most appropriate for the sample size and the structure of interest, organelles are characterised in 3D with more physiologically meaningful information such as volume and surface area, and their interactions within the surrounding cell and tissue environment.

3.3. *Focused-ion-beam scanning electron microscopy (FIB-SEM) tomography*

FIB technology was developed in the 1970s for semiconductor manufacturing and later applied for the preparation of thin sections (lamellae) for TEM [54]. However, it was not until 2006 that this technique was applied to study 3D cellular structure through tomography [55]. During, FIB-SEM tomography, the surface of the sample is imaged by SEM, and an ablative focused beam of gallium ions (Ga^{+}) is used to 'mill' away a thin section of the previously imaged surface [56]. In doing so, a new surface is exposed for imaging, and this process is repeated to produce an image series that can be reconstructed into a volume (Fig. 4A). While FIB-SEM tomography typically achieves a high resolution (~3–10 nm pixel size), excessive time for milling samples limits the technique's application to imaging small volumes [57,58]. While promising, FIB-SEM tomography has not yet been applied to study human trophoblast ultrastructure, however, the technique was applied to examine bovine and porcine microvillous junctions [59]. This study compared distinct structural features of placentae between species, which would not be possible using standard 2D electron microscopy techniques.

In the context of subcellular organelles, FIB-SEM has primarily been applied to study mitochondrial structure within mouse heart and brain [60,61]. These studies have demonstrated how mitochondrial structure underpins respiratory and metabolic function, by supporting structural insights from FIB-SEM with respiratory data via Seahorse XF (Agilent Technologies, USA) [60,61]. Furthermore, 3D reconstruction techniques have improved our understanding of the formation of mitochondrial networks via fusion and fission processes, mediated by the mitochondrial dynamics proteins. Of these proteins, the role of dynamin-related protein 1 (DRP1) in constricting and separating mitochondria into separate organelles has been confirmed via FIB-SEM reconstruction [60,62]. To support visual observations and 3D reconstructions, the development of methods for the quantitative assessment of 3D reconstructions have permitted statistical comparisons of mitochondrial volumetrics, showcasing the spectrum of structural organisation between branched and isolated mitochondrial morphologies in porcine cells [45]. More recent advances in this technique have permitted the use of correlative light and electron microscopy (CLEM), which enables the localisation of specific ultrastructures and proteins using fluorescent antibodies [63]. As with electron microscopy, CLEM enables detailed ultrastructural analysis using electrons, while also housing a fluorescence microscope to detect immunolabelled regions of interest within the sample [64]. When these imaging modalities are combined, ultrastructural insights can be localised to specific proteins of interest, including the presence of the cleavage protein DRP1 [63]. However, as reported by *Ohta* et al., incorporating CLEM is technically challenging due to the complexity of the sample preparation, and alignment of both imaging modes [63]. Few examples exist in which mitochondrial cristae have been resolved using FIB-SEM tomography, and while gross cristae morphology may be determined, it is exceedingly difficult to analyse tight regions of the intermembrane space and lamellar cristae [65–67]. However, a notable example of this is a study by *Hu* et al., who used FIB-SEM tomography to examine the process of cristae formation and organisation [66].

An example of a milled lamella, which we produced using FIB-SEM of high-pressure frozen human placental tissue for the purpose of cryo-ET, has been included to demonstrate this technique (Fig. 4B–D). However, this acquisition proved unsuccessful due to the density and thickness of the tissue, which was too thick for efficient gallium ion milling, and led to lengthy milling time and excessive tissue damage due to charging [68]. This major limitation has restricted the field to preparing lamellae

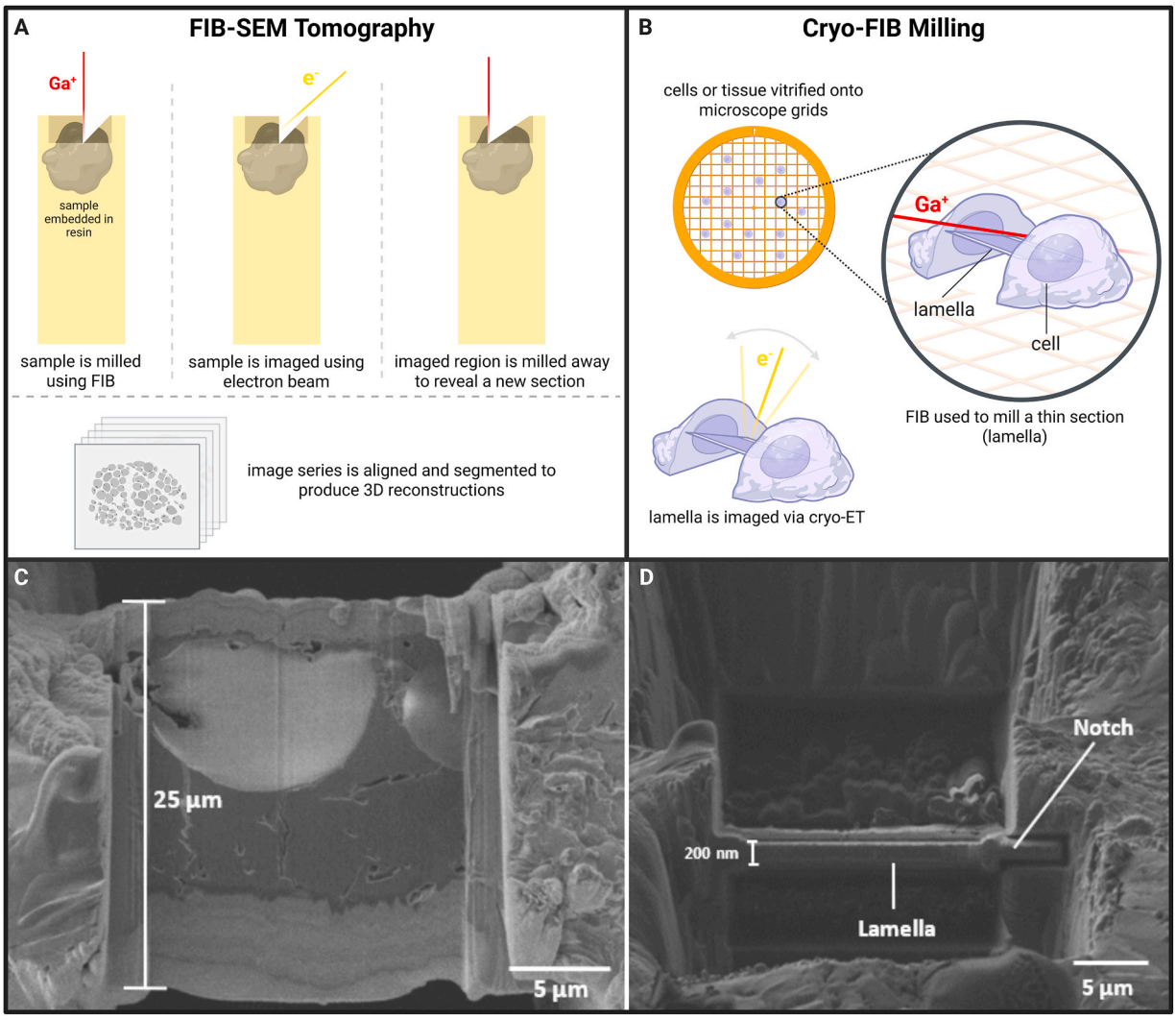

Fig. 4. Using FIB-SEM to reveal cellular ultrastructure. A) Overview of FIB-SEM tomography, in which samples are embedded in resin and milled using gallium ions. As the surface of the sample is exposed, electrons are used to acquire images via backscatter detectors. After imaging, the FIB is used again to mill away the region and reveal a new section within the volume. The images are aligned into a series and can be segmented to produce 3D reconstructions. B) Overview of cryo-FIB milling to produce lamellae (thin sections of sample) suitable for 3D reconstruction by cryo-ET. C) Top-down view of lamella FIB-milled from high-pressure frozen human placental tissue, and D) milling angle (in-line with the lamella) reveals a notch that relieves structural stress and tension. Scale bars represent 5 µm.

from plunge-frozen animal and human cells, isolated organelles such as mitochondria and extracellular vesicles, large bacteria, and microbes instead of tissue. Growing accessibility and reduced cost of plasma FIB-SEM, which uses xenon plasma instead of gallium ions, should lead to a new standard for preparing tissue lamellae, enabling in situ organelle and protein structure determination within human tissues like the placenta [68,69].

3.4. *Serial block-face scanning electron microscopy (SBF-SEM)*

SBF-SEM was developed in 2004 as an alternative to FIB-SEM, and uses a diamond knife within the microscope to serially section through the volume instead of an ion beam (Fig. 5A) [70]. However, in contrast to the thin sections achieved by FIB-SEM, the thickness of section achieved by SBF-SEM is typically larger than that of FIB-SEM (~20–100 nm), and therefore limits the resolution in the Z-axis [71,72].

Unlike FIB-SEM, SBF-SEM has been used with great success in placental research, with its first application in 2020, which revealed the 3D structure of microvasculature and endothelial cells [73]. Specifically, by characterising endothelial junctions, trans-endothelial channels, and inter-endothelial protrusions, *Palaiologou* et al., revealed the structural mechanisms that underpin capillary permeability [73]. However, it was noted that a significant limitation of SBF-SEM was the cost of the technique, and the need for automated segmentation tools to reduce the time required for analysis [73]. SBF-SEM has also been used to quantify folds of the basement membrane and the subsequent increase in surface area available for exchange [74]. In 2023, SBF-SEM was applied to study villous trophoblasts, producing a 3D reconstruction of a CTB cell [44]. Similarly, a separate study by *Palaiologou* et al., used a 3D reconstruction of a stromal fibroblast within human placental villi, to show the complexity of interactions with surrounding capillaries and stromal extracellular macrovesicles [75]. Work by *Lewis* et al., has since revealed trans-syncytial nanopores across the STB, which serve as routes for paracellular diffusion [76]. Such insights would not be possible with conventional 2D imaging, due to the topological complexity of nanopores in the context of surrounding syncytial tissue. The importance of 3D imaging by SBF-SEM is highlighted by our 3D reconstruction of microvilli, which shows the topological complexity of the microvillous membrane, consistent with *Kazemian* et al.'s observations of bovine and porcine microvilli (Fig. 5B and C) [59].

SBF-SEM has also been used to reconstruct whole cells in other tissues, as demonstrated by *Wernitznig* et al., who examined the

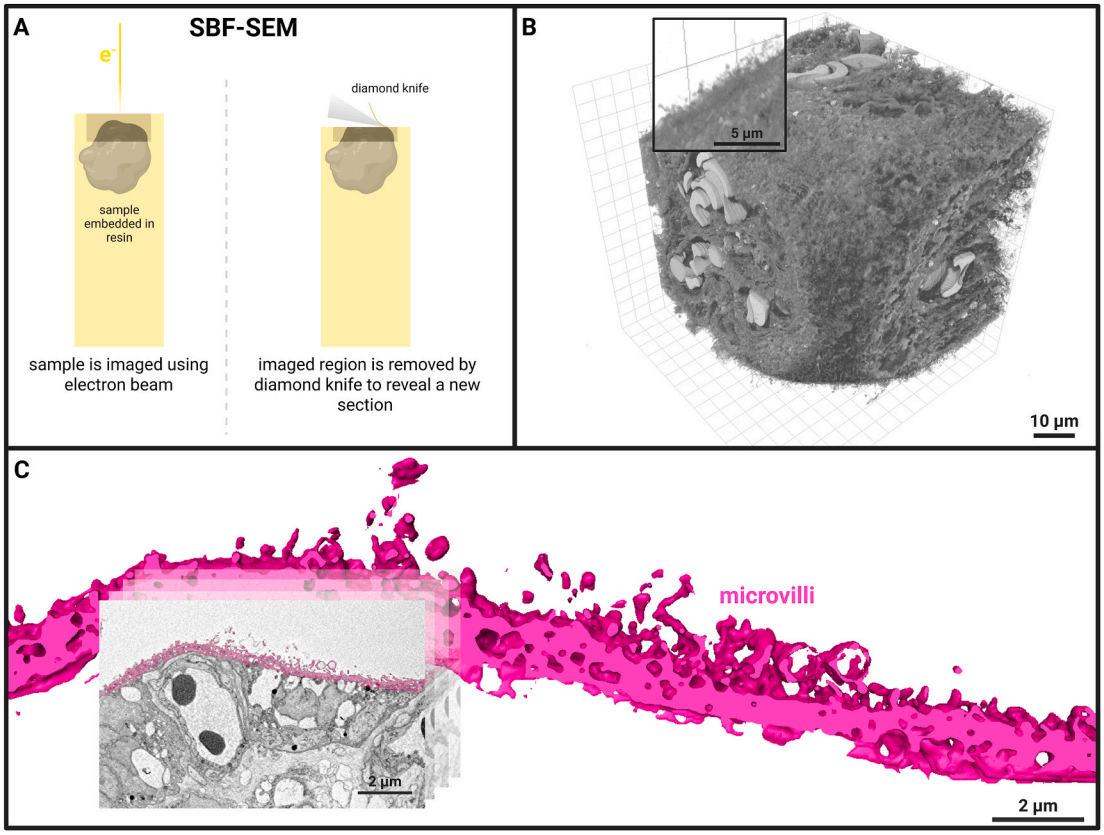

Fig. 5. Using SBF-SEM to reveal cellular ultrastructure. A) Overview of SBF-SEM, in which the surface of the sample is imaged by electrons and the imaged region is removed using a diamond knife, thereby revealing a new section within the volume. B) Human placental villi were fixed, stained, dehydrated, and embedded in resin prior to SBF-SEM. Images were aligned to produce a 3D reconstruction of placental villi, scale bar represents 10 µm. Magnified region shows microvilli on the surface of the STB, scale bar represents 5 µm. C) A representative region of microvilli of the STB was segmented for 3D reconstruction using Amira (Thermo Fisher Scientific, USA). Scale bars represent 2 µm.

morphology and intracellular connectivity between locust neurons [77]. Additionally, SBF-SEM has been used to map mitochondrial networks in human skeletal muscle tissue, quantifying network complexity using the mitochondrial complexity index (MCI) [78]. In this study, *Vincent* et al., report the existence of mitochondrial subpopulations, nanotunnels between mitochondria, as well as an association between the presence of mitochondrial DNA (mtDNA) defects and lower MCI in patients affected by mtDNA disease [78]. As a novel bridge between 3D imaging and quantitative analysis of structure, this study demonstrated the strength of SBF-SEM in gaining insights into mitochondrial dysfunction [78]. *Bleck* et al., have also used SBF-SEM to map mitochondrial connectivity across networks in skeletal and cardiac mouse tissue [79]. It was noted that mitochondrial networks had the capacity to self-organise and modulate the direction of inter-connectivity in relation to the axis of muscle contraction [79]. Moreover, the mitochondrial networks were quantitatively assessed across both glycolytic and oxidative muscle types [79]. In the placental field, *Lewis* et al., applied SBF-SEM to map mitochondria and the surrounding reticular networks within the CTB, and while this study did not quantitatively assess mitochondrial structure, it demonstrated the capacity of the technique to reveal placental organelles in 3D [44].

3.5. Array tomography

The most recently developed of the three primary volume electron microscopy techniques is array tomography, developed in 2007. Array tomography is a technique in which the sample is sectioned by an ultramicrotome (typically 30–80 nm thick), and sections are recovered onto glass or silicon slides in an ordered array (Fig. 6A and B) [80]. Subsequently, each of these sections are imaged by SEM and reconstructed into a 3D volume. Since sample is thin and in direct contact with conductive substrate that has been applied prior to imaging, there is less electron charging and therefore the technique can be used to image samples at higher resolution. Moreover, due to manual sectioning and choice of block size, larger sample volumes can be imaged, enabling better contextualisation of placental cells within the surrounding villous tissue structure in 3D (Fig. 6C and D) [81]. Given that each section may tolerate a higher electron dose, array tomography is suitable for resolving the structure of various placental organelles including mitochondria of the CTB (Fig. 6E) and STB (Fig. 6F), extracellular vesicles (Fig. 6G), and extracellular matrix fibres (Fig. 6H). Furthermore, it is possible to stain sections with fluorescent antibodies prior to imaging and conduct CLEM, for unambiguous structure localisation and visualisation of protein abundance [80].

Like SBF-SEM, array tomography has been used to study the human placenta, producing 3D reconstructions of CTBs and the STB [7]. While 2D imaging presents CTBs as cuboidal with straight interfaces along the basement membrane, *Acharya* et al., used array tomography to show that it is common for the basement membrane to wrap around elongated cellular projections of the CTB in the term placenta [7]. In addition to cellular morphology, our recent research has investigated the 3D network structure of mitochondria within CTBs and the STB by incorporating the aforementioned MCI, building upon previous 2D observations of mitochondrial morphology by quantitatively comparing

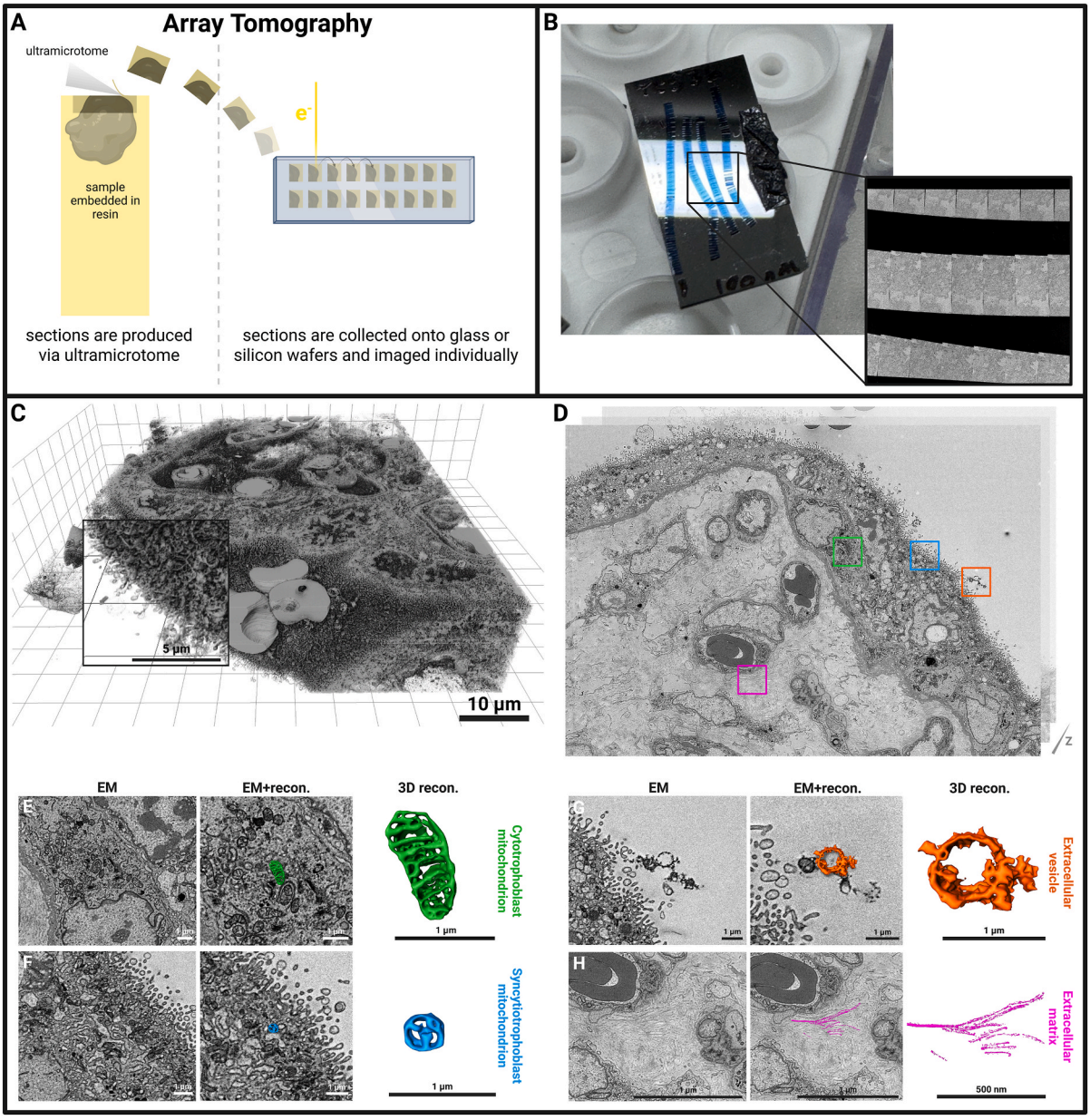

Fig. 6. Using array tomography to resolve placental organelles in 3D. A) Overview of array tomography, in which the resin-embedded sample is sectioned by ultramicrotome, and sections are collected onto glass or silicon wafers. Each section is then individually imaged by SEM to produce an image series. B) Ribbons of sections on a silicon wafer, with the magnified region showing an overview of the sections acquired by SEM. C) Placental tissue was fixed, stained, dehydrated, and embedded in resin for array tomography, to produce a 3D reconstruction of the tissue, scale bar represents 10 µm. The magnified region shows extensive detail of the microvillous surface, scale bar represents 5 µm. D) Representative images from the image series, showing organelles and ultrastructural features identified as Cyto-Mito (green square), Syncytio-Mito (blue square), extracellular vesicle (orange square), and extracellular matrix fibres (pink square). E) Magnified images of Cyto-Mito with lamellar cristae architecture, F) Syncytio-Mito with tubulo-vesicular cristae architecture, G) extracellular vesicle decorated with surface protein structures, and H) extracellular matrix fibres. Presented are the electron microscopy images (EM), the image with the 3D reconstruction (EM + recon.), and isolated 3D reconstructions (3D recon.). Scale bar represents 500 nm for the reconstruction of extracellular matrix fibres, all other scale bars represent 1 µm.

elongated Cyto-Mitos and spherical Syncytio-Mitos [7]. Our study also highlights the advantage of combining 3D imaging modalities with fundamental proteomic analysis, improving our understanding of the links between mitochondrial structure and the underlying mechanisms that govern structure, in a similar way to the insights provided by the gold immunolabelled 2D imaging of *Martinez* et al. [7,38]. Indeed, we combined array tomography with liquid chromatography-mass spectrometry (LC-MS) to interrogate the proteins involved in mitochondrial fusion and network formation in the CTB, in contrast with fission and fragmentation in the surrounding STB despite being 600 nm apart [7]. These findings seemingly confirm that the differentiation of CTBs into the STB is accompanied by the remodelling of mitochondrial network structure, building upon the work of *Martinez* et al., *Kolahi* et al., and *Fisher* et al. [6,7,38,42]. Moreover, these data suggest that loss of mitochondrial membrane fusion proteins mitofusin 1 (MFN1) and optic atrophy 1 (OPA1), and increase in cleavage protein DRP1 in the STB, leads to a fragmented and smaller mitochondrial network [7]. The role of these mitochondrial dynamics proteins in mediating network structure has been suggested in the placenta from 2D electron microscopy and have been shown to be disrupted in placental pathologies including preeclampsia and gestational diabetes mellitus [48,61,62,82–84]. Collectively, the use of array tomography supports previous findings

pertaining to the remodelling of mitochondrial structure following CTB fusion, suggesting that this structural adaptation is necessary for accommodating reduced bioenergetic demands and elevated steroid hormone synthesis in the STB [6,7,38,42].

Further advances in array tomography have been made in other tissues, such as the work of *Kay* et al., who used array tomography to produce immunofluorescence and electron micrographs of synapses in the human brain, including the size and distribution of neuronal mitochondria [85]. While the difficulty of the procedure was noted by the authors, this study demonstrated the benefit of combining imaging modalities to assess both structural and functional aspects of human tissue [85]. Perhaps the most notable example of array tomography in recent years, is the landmark study by *Shapson-Coe* et al., in which a 1 mm^3 fragment of human cerebral cortex was resolved with a resolution of 4 nm [86]. To achieve this, sections were collected on an automated continuous tape instead of a glass or silicon wafer, a technique known as automated tape-collecting ultramicrotome SEM (ATUM-SEM) [86]. By using a flood-filling network (class of neural network designed for segmentation of complex shapes), *Shapson-Coe* et al., were able to reconstruct 57,000 cells, and around 150 million synapses, from 1.4 petabytes of data [86]. By exploring 3D ultrastructure, the authors of this work were able to discover a previously unrecognised class of directionally oriented neurons, which revealed the complexity of synaptic connections between neurons throughout the tissue [86]. Moreover, the use of machine learning techniques demonstrates the feasibility of high throughput image analysis and classification of large volume data, which has been the primary rate-limiting step of volume electron microscopy thus far [86].

4. Applications of cryo-electron microscopy

4.1. From 3D to resolving structure at Angstrom-resolution: determining in situ protein structure

Cryo-electron microscopy (cryo-EM) has primarily been used to study isolated and purified protein samples through single particle analysis (SPA), through which hundreds of thousands of randomly orientated proteins or viruses are vitrified on grids, imaged, aligned, and combined reveal 3D protein structure (Fig. 7A) [87]. However, the emergence of cryogenic electron tomography (cryo-ET) has enabled the determination of in situ protein structure within the native membrane environment (Fig. 7B) [88]. As such, given the role of mitochondrial protein complexes in governing cristae curvature, cryo-ET has the potential to revolutionise our understanding of structure-to-function relationships [89,90]. The high resolution achieved by cryo-ET, is in part due to the absence of chemical fixatives (which limit resolution and increase image noise). Therefore, fresh samples must be preserved in amorphous ice onto electron microscopy grids, through a process called vitrification [91]. This process is typically achieved using a plunge-freezing device, which rapidly submerges the sample into liquid ethane and avoids the formation of ice crystals (a major contaminant in cryo-EM) [91]. Since the cryo-EM operates at cryogenic temperature (−180 °C), samples cannot be thawed at any time and must be stored in liquid nitrogen from the point of vitrification. To reach ultimate resolution, cryo-ET typically requires samples to be ultrathin (10–100 nm) for improved contrast and reduced noise, therefore thicker samples like cells must be thinned using a FIB-SEM prior to data collection [92,93]. Smaller samples, including isolated organelles like mitochondria, may be imaged after vitrification and is a potential avenue when access to a FIB-SEM is limited [7,94].

To perform cryo-ET, samples are tilted (typically ± 60°) within a high-resolution cryoTEM, which collects electron micrographs during this process [95]. Micrographs are then aligned to produce a tomographic reconstruction (tomogram), which is used for the segmentation of biological membranes. From this data, in situ protein structure may also be determined using subtomogram averaging, a process where macromolecular particles are identified (either automatically using template matching and machine learning, or manually) and cropped into subvolumes [96]. The individual subvolumes, which contain randomly aligned macromolecules, are then aligned and averaged to form a refined 3D protein structure that can be mapped back to their native environment within the membrane (Fig. 7B) [96]. Subtomogram averaging is yet to be applied to resolve placental protein structure, presenting the field with the opportunity to gain an advanced understanding of the structural and functional mechanisms underpinning placental development and pathology.

4.2. Cryo-ET, the forefront of mitochondrial imaging; studying mitochondrial cristae and the electron transport chain using subtomogram averaging

The continued application of cryo-ET and transition from isolated protein SPA to subtomogram averaging, has been used to great effect in other fields. Notably, *Davies* et al., resolved mitochondrial cristae architecture and localised ATP synthase dimers along highly curved membrane ridges and apices in yeast and fungal cells [97]. This study was crucial in establishing the role of ATP synthase in shaping cristae, and has since been supported by studies of a wide range of parasitic, yeast, fungal, plant, and animal cells, all of which used cryo-ET [89,90,94,98–100].

Following the initial applications of subtomogram averaging, improved pipelines for particle-picking and structure averaging has now revealed the presence of supercomplexes, which are higher-order assemblies of the electron transport chain typically in configurations of complexes I + III + IV or III + IV. The existence of various supercomplex stoichiometries have now been revealed using cryo-ET, such as I + II + III_2+IV_2, I + III_2+IV_2, I_2+III_2+IV_2, and I_2+III_4+IV_2, some of which are only observed in vivo [101,102]. In a manner similar to ATP synthase, supercomplexes have also been shown to induce membrane curvature, indicating that cristae architecture is governed not only by mitochondrial cristae organisation proteins (MICOS), but also by the electron transport chain itself [67,103,104]. Moreover, other cryo-ET studies have confirmed the role of abnormal cristae architecture in human disease such as Leigh syndrome, and investigated the role of OPA1 in governing cristae architecture [105,106]. Despite this advanced understanding of supercomplex structure and function in unicellular microorganisms like *T. thermophila* and *Saccharomyces cerevisiae*, little is known about their presence in human tissues such as the placenta.

The first placental protein structure was resolved using cryo-EM and SPA, by isolating and purifying the protein calcium homeostasis modulator (CALHM) from primary cultures of human placental cells [107]. Although cryo-EM was used as opposed to cryo-ET (which would resolve in situ protein structure), this study revealed distinct conformational states of ion channels and their importance in mediating transport processes during fetal development [107]. The ability of cryo-ET to determine Angstrom-resolution information of internal mitochondrial architecture, has permitted the study of isolated mitochondria from the human placenta, revealing the presence of mitochondrial subpopulations in CTBs and the STB [7]. Moreover, each of the subpopulations observed had specific cristae architectures, with lamellar and tubulo-vesicular cristae in the CTB, and a homogenous globular population in the STB [7]. In this study, we propose that the remodelling of cristae architecture following CTB differentiation, through loss of MICOS, OPA1, and supercomplexes, is crucial for meeting lower bioenergetic demands and increased steroidogenic functions of the syncytium, therefore supporting the work of *Martinez* et al., *Kolahi* et al., and *Fisher* et al. [6,7,38,42]. However, it was noted that the density and thickness of vitrified, isolated mitochondria limited observations of membrane proteins [7]. Therefore, future studies of the placenta may improve image quality by preparing thinner samples by FIB-SEM milling, enabling protein structure determination by subtomogram averaging [7,68,69].

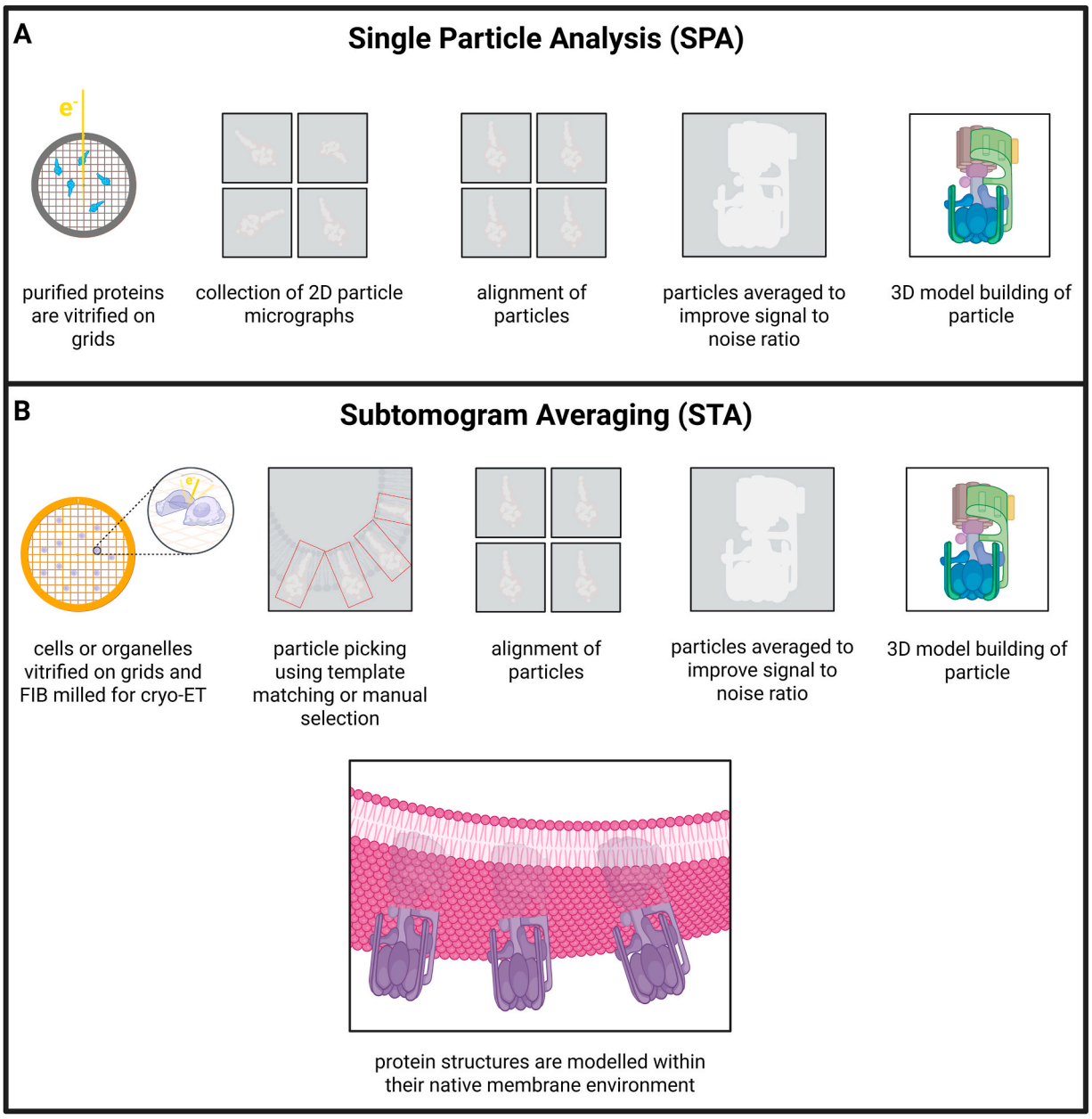

Fig. 7. Approaches for determining protein structure. A) Overview of the single particle analysis (SPA) workflow, in which proteins are isolated, purified, and vitrified on grids. Hundreds of thousands of particles are imaged via cryo-EM, followed by alignment, averaging, and 3D modelling of protein structure. B) Overview of the subtomogram averaging (STA) workflow, in which whole cells or organelles are vitrified on grids and FIB milled. The thin lamella is then imaged via cryo-ET, producing tilt series images of membranes and embedded proteins. Proteins of interest are picked either using template matching or manual selection, followed by alignment, averaging, and 3D modelling of the in situ protein structure. The structure is then modelled within the native membrane environment to assess the interactions between protein structure and morphology.

5. Addressing challenges and limitations

Despite the potential for 3D electron microscopy to drive our understanding of organelle structure and function, there remains several challenges and limitations that must be addressed. Access to sample preparation equipment and electron microscopes remains limited in many institutes, and this is particularly the case for cryo-ET which demands tools for vitrification and high-resolution microscopes. Due to high purchasing and maintenance costs, access to these microscopes remains limited in many countries around the world, particularly in low-middle income regions such as Africa, South and Southeast Asia, and South America [108,109].

Even with access to specialist equipment, it is clear that our capacity to produce high-resolution images and datasets far exceeds our ability to interpret such data into meaningful information [110]. Specifically, image segmentation is one of the largest limitations as it typically takes several weeks to months to segment and reconstruct organelles in large volume datasets. Moreover, while most electron microscopy image processing software is free, advanced image processing and analysis requires licensed software. Advances are being made in the field of machine learning and trainable computational tools for the detection of organelles and membranes, however, implementation in the context of the placenta may prove challenging as the tissue is dense and heterogenous [111]. Such challenges include the STB and the extensive diversity of organelle structure following trophoblast differentiation [7, 110]. Notably, MemBrain v2 (University of Munich, Germany) is

capable of segmenting cryo-ET membranes with relatively clean datasets, however at present, mesh holes are frequent and require manual repair [112]. Promisingly, electron microscopy data can be deposited within archives post-publication with the potential for training neural network models to recognise features within placental tissue including mitochondria and other organelles, overcoming this shortfall in time and with advances in computational power [113–115]. Perhaps the largest limitation of all, is that electron microscopy is an observation of a single moment in time, and is not capable of producing temporal information as can be achieved with live-cell microscopy. Some advances are being made in the application of time-resolved cryo-EM, demonstrated by *Bhattacharjee* et al., as a powerful technique for studying ribosome kinetics and intermediary protein conformations, albeit difficult due to the length of sample processing and computational limitations [116]. Therefore, the strength of electron microscopy is its collective use with other biological research techniques that reveal genomic, transcriptomic, and proteomic information with functional insights, to form a multimodal investigative strategy.

6. Future perspectives and conclusions

Despite the crucial role of the placenta in supporting fetal development, the trophoblast bilayer remains one of the least understood human tissues, given its exceeding complexity and extensive ultrastructural remodelling following CTB fusion. The placental research field has benefitted from the application of volume electron microscopy techniques such as SBF-SEM, and array tomography, which have resolved 3D organelle structure with remarkable context of the surrounding tissue environment. In addition to improving our understanding of trophoblast morphology, these volume electron microscopy techniques have offered novel insights into the ways mitochondrial structure adapts as CTBs fuse, forming a STB with reformed functional demands. Studies currently implementing these techniques to study the placenta offer a foundational physiological understanding by building upon previous 2D insights, and quantifying cellular and organelle interactions in 3D. Such techniques have also been used to great success in other tissues, showcasing workflows that provide both structural and functional insights through CLEM. Additionally, novel advances in the field of cryo-ET, such as subtomogram averaging, should be exploited in the placenta to understand the structural mechanisms and determine in situ protein structure. Moreover, many of the findings discussed in this review are yet to be assessed in pathology and pose the exciting prospect of uncovering the ultrastructural basis of placental dysfunction.

CRediT authorship contribution statement

Siddharth Acharya: Writing – original draft, Methodology, Conceptualization. **Eric Hanssen:** Writing – review & editing, Methodology. **James C. Bouwer:** Writing – review & editing, Methodology, Conceptualization. **John E. Schjenken:** Writing – review & editing, Writing – original draft, Conceptualization. **Kirsty G. Pringle:** Writing – review & editing, Writing – original draft, Conceptualization. **Roger Smith:** Writing – review & editing, Writing – original draft, Funding acquisition, Conceptualization. **Joshua J. Fisher:** Writing – review & editing, Writing – original draft, Funding acquisition, Conceptualization.

Ethical approval

Ethical approval was granted by the University of Newcastle Research Ethics Committee (H-382-0602), Hunter New England Health Human Research Ethics Committee (02/06/12/.13), Mercy Health Human Research Ethics Committee (R11/34), and Site Specific Assessment (SSA/15/HNE/291) in compliance with the Declaration of Helsinki standards. With informed written consent, placental samples for SBF-SEM, array tomography, and FIB-milling were collected from healthy full-term pregnancies (38–40 weeks) at the John Hunter Hospital (NSW, Australia) and Mercy Hospital for Women (VIC, Australia).

Declaration of competing interest

The authors declare that the research and was conducted in the absence of any commercial or financial relationships that could be construed as a potential competing interest.

Acknowledgements

We would like to acknowledge Dr. Boyin Liu, who assisted in the preparation of placental lamellae via FIB-SEM. We would also like to express our gratitude to the research midwives and clinical staff of the John Hunter Hospital and Mercy Hospital for Women, and to the patients who donated placentae for this research. Diagrammatic figures were created with BioRender.com.

References

[1] T. Napso, H.E.J. Yong, J. Lopez-Tello, A.N. Sferruzzi-Perri, The role of placental hormones in mediating maternal adaptations to support pregnancy and lactation, Front. Physiol. 9 (2018), 2018.
[2] J.D. Aplin, Developmental cell biology of human villous trophoblast: current research problems, Int. J. Dev. Biol. 54 (2–3) (2010) 323–329.
[3] M. Knöfler, S. Haider, L. Saleh, J. Pollheimer, T.K.J.B. Gamage, J. James, Human placenta and trophoblast development: key molecular mechanisms and model systems, Cell. Mol. Life Sci. 76 (18) (2019) 3479–3496.
[4] C.J.P. Jones, H. Fox, Ultrastructure of the normal human placenta, Electron. Microsc. Rev. 4 (1) (1991) 129–178.
[5] J.D. Boyd, W.J. Hamilton, Electron microscopic observations on the cytotrophoblast contribution to the syncytium in the human placenta, J. Anat. 100 (Pt 3) (1966) 535–548.
[6] J. Fisher, D. McKeating, E. Pennell, J. Cuffe, O. Holland, A. Perkins, Mitochondrial isolation, cryopreservation and preliminary biochemical characterisation from placental cytotrophoblast and syncytiotrophoblast, Placenta 82 (2019) 1–4.
[7] S. Acharya, E. Hanssen, V.B. Botha, T.M. Smith, S. Jayatissa, Z. Trifunovic, L. A. Bartho, J.E. Schjenken, T.u.J. Kaitu'u-Lino, A.V. Perkins, J.L. James, K. G. Pringle, J.C. Bouwer, R. Smith, J.J. Fisher, Electron tomography reveals mitochondrial network and cristae remodelling during cell differentiation in the human placenta, bioRxiv 2025 (2025), 06.09.658204.
[8] L. Marton, The electron microscope: a new tool for bacteriological research, J. Bacteriol. 41 (3) (1941) 397–413.
[9] A. Ryabov, P. Baum, Electron microscopy of electromagnetic waveforms, Science 353 (6297) (2016) 374–377.
[10] A.V. Crewe, D.N. Eggenberger, J. Wall, L.M. Welter, Electron Gun using a field emission source, Rev. Sci. Instrum. 39 (4) (1968) 576–583.
[11] W.B. Nottingham, Thermionic Emission, Electron-Emission Gas Discharges I/ Elektronen-Emission Gasentladungen I, Springer Berlin Heidelberg, Berlin, Heidelberg, 1956, pp. 1–175.
[12] D.A. Muller, Structure and bonding at the atomic scale by scanning transmission electron microscopy, Nat. Mater. 8 (4) (2009) 263–270.
[13] J. Seiter, E. Müller, H. Blank, H. Gehrke, D. Marko, D. Gerthsen, Backscattered electron SEM imaging of cells and determination of the information depth, J. Microsc. 254 (2) (2014) 75–83.
[14] M. Bárcena, A.J. Koster, Electron tomography in life science, Semin. Cell Dev. Biol. 20 (8) (2009) 920–930.
[15] C.J. Peddie, C. Genoud, A. Kreshuk, K. Meechan, K.D. Micheva, K. Narayan, C. Pape, R.G. Parton, N.L. Schieber, Y. Schwab, B. Titze, P. Verkade, A. Weigel, L. M. Collinson, Volume electron microscopy, Nat. Rev. Methods Primers 2 (1) (2022) 51.
[16] W. Baumeister, Cryo-electron tomography: a long journey to the inner space of cells, Cell 185 (15) (2022) 2649–2652.
[17] J.L. Dickerson, K. Naydenova, M.J. Peet, H. Wilson, B. Nandy, G. McMullan, R. Morrison, C.J. Russo, Reducing the effects of radiation damage in cryo-EM using liquid helium temperatures, Proc. Natl. Acad. Sci. 122 (17) (2025) e2421538122.
[18] M. Marko, C. Hsieh, R. Schalek, J. Frank, C. Mannella, Focused-ion-beam thinning of frozen-hydrated biological specimens for cryo-electron microscopy, Nat. Methods 4 (3) (2007) 215–217.
[19] E.W. Dempsey, Electron microscopy of the visceral yolksac epithelium of the Guinea pig, Am. J. Anat. 93 (3) (1953) 331–363.

[20] E. Dempsey, G. Wislocki, Electron microscopy of human placental villi, Anat. Rec. 117 (1953) 609.
[21] G.B. Wislocki, E.W. Dempsey, Electron microscopy of the human placenta, Anat. Rec. 123 (2) (1955) 133–167.
[22] J.D. Boyd, A.F. Hughes, Observations on human chorionic villi using the electron microscope, J. Anat. 88 (3) (1954) 356–362.
[23] M. Haider, S. Uhlemann, E. Schwan, H. Rose, B. Kabius, K. Urban, Electron microscopy image enhanced, Nature 392 (6678) (1998) 768–769.
[24] Y. Harada, T. Tomita, Y. Kokubo, H. Daimon, S. Ino, Development of an ultrahigh vacuum high resolution scanning transmission electron microscope, J. Electron. Microsc. 42 (5) (1993) 294–304.
[25] F.A. Hamm, A lapping technique: to improve the image quality of electron microscope lenses, J. Appl. Phys. 21 (4) (1950) 271–278.
[26] B.E. Bammes, R.H. Rochat, J. Jakana, W. Chiu, Practical performance evaluation of a 10k×10k CCD for electron cryo-microscopy, J. Struct. Biol. 175 (3) (2011) 384–393.
[27] J.F. Hamilton, J.C. Marchant, Image recording in Electron Microscopy, J. Opt. Soc. Am. 57 (2) (1967) 232–239.
[28] E. Zeitler, The photographic emulsion as analog recorder for electrons, Ultramicroscopy 46 (1) (1992) 405–416.
[29] H. Brown, J. Baker, W. Cybulski, A. Fenton, J. Glover, P. Negus, J. Palm, The role of microfilm in digital preservation, Microform & Digitization Rev. 41 (2) (2012) 65–82.
[30] C.R. Booth, J. Jakana, W. Chiu, Assessing the capabilities of a 4kx4k CCD camera for electron cryo-microscopy at 300kV, J. Struct. Biol. 156 (3) (2006) 556–563.
[31] A. Horstmann, S. Riggs, Y. Chaban, D.K. Clare, G. de Freitas, D. Farmer, A. Howe, K.L. Morris, D. Hatton, A service-based approach to cryoEM facility processing pipelines at eBIC, Acta Crystallogr D Struct Biol 80 (Pt 3) (2024) 174–180.
[32] E.W. Dempsey, Variations in the structure of mitochondria, J. Biophys. Biochem. Cytol. 2 (4) (1956) 305–312.
[33] T. Wakitani, Electronmicroscopic observation on the chorionic villi of the normal human placenta and chorioepithelioma maligunum, 1, J. Jpn. Obstet. Gynecol. Soc. 8 (3) (1961).
[34] W.J. Hamilton, J.D. Boyd, Development of the human placenta in the first three months of gestation, J. Anat. 94 (Pt 3) (1960) 297–328.
[35] M. Castellucci, P. Kaufmann, A three-dimensional study of the normal human placental villous core: II. Stromal architecture, Placenta 3 (3) (1982) 269–285.
[36] G.J. Burton, The fine structure of the human placental villus as revealed by scanning electron microscopy, Scanning Microsc. 1 (4) (1987) 1811–1828.
[37] B.J. Martin, S.S. Spicer, Multivesicular bodies and related structures of the syncytiotrophoblast of human term placenta, Anat. Rec. 175 (1) (1973) 15–35.
[38] F. Martínez, M. Kiriakidou, J.F. Strauss III, Structural and functional changes in Mitochondria associated with trophoblast differentiation: methods to isolate enriched preparations of Syncytiotrophoblast Mitochondria, Endocrinology 138 (5) (1997) 2172–2183.
[39] E. Hanssen, C. Dekiwadia, D.T. Riglar, M. Rug, L. Lemgruber, A.F. Cowman, M. Cyrklaff, M. Kudryashev, F. Frischknecht, J. Baum, S.A. Ralph, Electron tomography of Plasmodium falciparum merozoites reveals core cellular events that underpin erythrocyte invasion, Cell. Microbiol. 15 (9) (2013) 1457–1472.
[40] J.A. Terzakis, The ultrastructure of normal human first trimester placenta, J. Ultra. Res. 9 (3) (1963) 268–284.
[41] J.R. Tighe, P.R. Garrod, R.C. Curran, The trophoblast of the human chorionic villus, J. Pathol. Bacteriol. 93 (2) (1967) 559–567.
[42] K.S. Kolahi, A.M. Valent, K.L. Thornburg, Cytotrophoblast, not syncytiotrophoblast, dominates glycolysis and oxidative phosphorylation in human term placenta, Sci. Rep. 7 (1) (2017) 42941.
[43] B.C. Jenkins, K. Neikirk, P. Katti, S.M. Claypool, A. Kirabo, M.R. McReynolds, A. Hinton Jr., Mitochondria in disease: changes in shapes and dynamics, Trends Biochem. Sci. 49 (4) (2024) 346–360.
[44] R.M. Lewis, Volume electron microscopy reveals placental ultrastructure in 3D, Placenta 141 (2023) 78–83.
[45] A. Lounas, A. Lebrun, I. Laflamme, N. Vernoux, J. Savage, M.-È. Tremblay, M. Germain, F.J. Richard, A 3D analysis revealed complexe mitochondria morphologies in porcine cumulus cells, Sci. Rep. 12 (1) (2022) 15403.
[46] A.E. Vincent, Y.S. Ng, K. White, T. Davey, C. Mannella, G. Falkous, C. Feeney, A. M. Schaefer, R. McFarland, G.S. Gorman, R.W. Taylor, D.M. Turnbull, M. Picard, The spectrum of mitochondrial ultrastructural defects in mitochondrial myopathy, Sci. Rep. 6 (1) (2016) 30610.
[47] O. Holland, M. Dekker Nitert, L.A. Gallo, M. Vejzovic, J.J. Fisher, A.V. Perkins, Review: placental mitochondrial function and structure in gestational disorders, Placenta 54 (2017) 2–9.
[48] L. Tilokani, S. Nagashima, V. Paupe, J. Prudent, Mitochondrial dynamics: overview of molecular mechanisms, Essays Biochem. 62 (3) (2018) 341–360.
[49] W. Chen, H. Zhao, Y. Li, Mitochondrial dynamics in health and disease: mechanisms and potential targets, Signal Transduct. Targeted Ther. 8 (1) (2023) 333.
[50] A.M. Seligman, H.L. Wasserkrug, J.S. Hanker, A new staining method (OTO) for enhancing contrast of lipid–containing membranes and droplets in osmium tetroxide–fixed tissue with osmiophilic thiocarbohydrazide(TCH), J. Cell Biol. 30 (2) (1966) 424–432.
[51] M.C. Willingham, A.V. Rutherford, The use of osmium-thiocarbohydrazide-osmium (OTO) and ferrocyanide-reduced osmium methods to enhance membrane contrast and preservation in cultured cells, J. Histochem. Cytochem. 32 (4) (1984) 455–460.
[52] A. Velazco, T. Glen, S. Klumpe, A. Pennington, J. Zhang, J.L.R. Smith, C. Glynn, W. Bowles, M. Kobylynska, R.A. Fleck, J.H. Naismith, J.S. Kim, M.C. Darrow, M. Grange, A.I. Kirkland, M. Dumoux, Reduction of SEM charging artefacts in native cryogenic biological samples, Nat. Commun. 16 (1) (2025) 5204.
[53] V. Baena, R.L. Schalek, J.W. Lichtman, M. Terasaki, Serial-section electron microscopy using automated tape-collecting ultramicrotome (ATUM), Methods Cell Biol. 152 (2019) 41–67.
[54] J. Orloff, High-resolution focused ion beams, Rev. Sci. Instrum. 64 (5) (1993) 1105–1130.
[55] J.A. Heymann, M. Hayles, I. Gestmann, L.A. Giannuzzi, B. Lich, S. Subramaniam, Site-specific 3D imaging of cells and tissues with a dual beam microscope, J. Struct. Biol. 155 (1) (2006) 63–73.
[56] S. Ch, R.R. Lim, S.W.Y. Low, D.G. Grant, S. Patterson, A. Ramasubramanian, A. K. Gadicherla, S.S. Chaurasia, A comprehensive overview of focused ion beam-scanning electron microscopy (FIB-SEM) applications for the evaluation of outer retina, Front. Cell Dev. Biol. 13 (2025) 1586029.
[57] C.S. Xu, K.J. Hayworth, Z. Lu, P. Grob, A.M. Hassan, J.G. García-Cerdán, K. K. Niyogi, E. Nogales, R.J. Weinberg, H.F. Hess, Enhanced FIB-SEM systems for large-volume 3D imaging, eLife 6 (2017).
[58] G. Knott, H. Marchman, D. Wall, B. Lich, Serial section scanning electron microscopy of adult brain tissue using focused ion beam milling, J. Neurosci. 28 (12) (2008) 2959–2964.
[59] A. Kazemian, R. Hooshmandabbasi, E.M. Schraner, A. Boos, K. Klisch, Evolutionary implications of fetal and maternal microvillous surfaces in epitheliochorial placentae, J. Morphol. 280 (4) (2019) 615–622.
[60] J. Heinen-Weiler, M. Hasenberg, M. Heisler, S. Settelmeier, A.L. Beerlage, H. Doepper, B. Walkenfort, A. Odersky, P. Luedike, E. Winterhager, T. Rassaf, U. B. Hendgen-Cotta, Superiority of focused ion beam-scanning electron microscope tomography of cardiomyocytes over standard 2D analyses highlighted by unmasking mitochondrial heterogeneity, J Cachexia Sarcopenia Muscle 12 (4) (2021) 933–954.
[61] H. Tamada, S. Kiryu-Seo, H. Hosokawa, K. Ohta, N. Ishihara, M. Nomura, K. Mihara, K.-i. Nakamura, H. Kiyama, Three-dimensional analysis of somatic mitochondrial dynamics in fission-deficient injured motor neurons using FIB/SEM, J. Comp. Neurol. 525 (11) (2017) 2535–2548.
[62] S.Y. Choi, J.Y. Kim, H.W. Kim, B. Cho, H.M. Cho, R.W. Oppenheim, H. Kim, I. J. Rhyu, W. Sun, Drp1-mediated mitochondrial dynamics and survival of developing chick motoneurons during the period of normal programmed cell death, Faseb j 27 (1) (2013) 51–62.
[63] K. Ohta, S. Hirashima, Y. Miyazono, A. Togo, K.-i. Nakamura, Correlation of organelle dynamics between light microscopic live imaging and electron microscopic 3D architecture using FIB-SEM, Microscopy 70 (2) (2020) 161–170.
[64] P. Ronchi, G. Mizzon, P. Machado, E. D'Imprima, B.T. Best, L. Cassella, S. Schnorrenberg, M.G. Montero, M. Jechlinger, A. Ephrussi, M. Leptin, J. Mahamid, Y. Schwab, High-precision targeting workflow for volume electron microscopy, JCB (J. Cell Biol.) 220 (9) (2021).
[65] C. Wang, L. Østergaard, S. Hasselholt, J. Sporring, A semi-automatic method for extracting mitochondrial cristae characteristics from 3D focused ion beam scanning electron microscopy data, Commun. Biol. 7 (1) (2024) 377.
[66] C. Hu, L. Shu, X. Huang, J. Yu, l. Li, L. Gong, M. Yang, Z. Wu, Z. Gao, Y. Zhao, L. Chen, Z. Song, OPA1 and MICOS Regulate mitochondrial crista dynamics and formation, Cell Death Dis. 11 (10) (2020) 940.
[67] T. Stephan, C. Brüser, M. Deckers, A.M. Steyer, F. Balzarotti, M. Barbot, T.S. Behr, G. Heim, W. Hübner, P. Ilgen, F. Lange, D. Pacheu-Grau, J.K. Pape, S. Stoldt, T. Huser, S.W. Hell, W. Möbius, P. Rehling, D. Riedel, S. Jakobs, MICOS assembly controls mitochondrial inner membrane remodeling and crista junction redistribution to mediate cristae formation, EMBO J. 39 (14) (2020) e104105.
[68] M. Dumoux, T. Glen, J.L.R. Smith, E.M.L. Ho, L.M.A. Perdigão, A. Pennington, S. Klumpe, N.B.Y. Yee, D.A. Farmer, P.Y.A. Lai, W. Bowles, R. Kelley, J.M. Plitzko, L. Wu, M. Basham, D.K. Clare, C.A. Siebert, M.C. Darrow, J.H. Naismith, M. Grange, Cryo-plasma FIB/SEM volume imaging of biological specimens, eLife 12 (2023).
[69] B.C. Creekmore, K. Kixmoeller, B.E. Black, E.B. Lee, Y.-W. Chang, Ultrastructure of human brain tissue vitrified from autopsy revealed by cryo-ET with cryo-plasma FIB milling, Nat. Commun. 15 (1) (2024) 2660.
[70] W. Denk, H. Horstmann, Serial block-face scanning electron microscopy to reconstruct three-dimensional tissue nanostructure, PLoS Biol. 2 (11) (2004) e329.
[71] J.A. Courson, P.T. Landry, T. Do, E. Spehlmann, P.J. Lafontant, N. Patel, R. E. Rumbaut, A.R. Burns, Serial block-face scanning electron microscopy (SBF-SEM) of biological tissue samples, J. Vis. Exp. 169 (2021).
[72] B. Chen, M. Yusuf, T. Hashimoto, A.K. Estandarte, G. Thompson, I. Robinson, Three-dimensional positioning and structure of chromosomes in a human prophase nucleus, Sci. Adv. 3 (7) (2017) e1602231.
[73] E. Palaiologou, P. Goggin, D.S. Chatelet, R. Ribeiro de Souza, W. Chiu, B. Ashley, E.M. Lofthouse, B.G. Sengers, C. Torrens, A.M. Page, J.K. Cleal, R.M. Lewis, Serial block-face scanning electron microscopy reveals novel intercellular connections in human term placental microvasculature, J. Anat. 237 (2) (2020) 241–249.
[74] S.A. Tashev, D. Parsons, C. Hillman, S. Harris, E.M. Lofthouse, P. Goggin, D. S. Chatelet, J.K. Cleal, N. Smyth, H. Palaiologou, A. Page, R.M. Lewis, Folding of the syncytiotrophoblast basal plasma membrane increases the surface area available for exchange in human placenta, Placenta 117 (2022) 57–63.
[75] E. Palaiologou, O. Etter, P. Goggin, D.S. Chatelet, D.A. Johnston, E.M. Lofthouse, R. Doherty, J. Pearson-Farr, B.G. Sengers, C. Torrens, J.K. Cleal, A.M. Page, R. M. Lewis, Human placental villi contain stromal macrovesicles associated with networks of stellate cells, J. Anat. 236 (1) (2020) 132–141.
[76] R.M. Lewis, H. Baskaran, J. Green, S. Tashev, E. Palaiologou, E.M. Lofthouse, J. K. Cleal, A. Page, D.S. Chatelet, P. Goggin, B.G. Sengers, 3D visualization of trans-

syncytial nanopores provides a pathway for paracellular diffusion across the human placental syncytiotrophoblast, iScience 25 (12) (2022).
[77] S. Wernitznig, F.C. Rind, A. Zankel, E. Bock, D. Gütl, U. Hobusch, M. Nikolic, L. Pargger, E. Pritz, S. Radulović, M. Sele, S. Summerauer, P. Pölt, G. Leitinger, The complex synaptic pathways onto a looming-detector neuron revealed using serial block-face scanning electron microscopy, J. Comp. Neurol. 530 (2) (2022) 518–536.
[78] A.E. Vincent, K. White, T. Davey, J. Philips, R.T. Ogden, C. Lawless, C. Warren, M. G. Hall, Y.S. Ng, G. Falkous, T. Holden, D. Deehan, R.W. Taylor, D.M. Turnbull, M. Picard, Quantitative 3D mapping of the human skeletal muscle mitochondrial network, Cell Rep. 26 (4) (2019) 996–1009, e4.
[79] C.K.E. Bleck, Y. Kim, T.B. Willingham, B. Glancy, Subcellular connectomic analyses of energy networks in striated muscle, Nat. Commun. 9 (1) (2018) 5111.
[80] K.D. Micheva, S.J. Smith, Array tomography: a new tool for imaging the molecular architecture and ultrastructure of neural circuits, Neuron 55 (1) (2007) 25–36.
[81] I. Kolotuev, Work smart, not hard: how array tomography can help increase the ultrastructure data output, J. Microsc. 295 (1) (2024) 42–60.
[82] J. Long, Y. Huang, Z. Tang, Y. Shan, D. Feng, W. Wang, J. Liu, Y. Huang, H. Gu, D. Guo, R. Yao, X. Ni, Mitochondria targeted antioxidant significantly alleviates Preeclampsia caused by 11β-HSD2 dysfunction via OPA1 and MtDNA maintenance, Antioxidants 11 (8) (2022).
[83] C. Voros, S. Stavros, I. Sapantzoglou, D. Mavrogianni, M.A. Daskalaki, M. Theodora, P. Antsaklis, P. Drakakis, D. Loutradis, G. Daskalakis, The role of placental mitochondrial dysfunction in adverse perinatal outcomes: a systematic review, J. Clin. Med. 14 (11) (2025).
[84] J.J. Fisher, C.L. Vanderpeet, L.A. Bartho, D.R. McKeating, J.S.M. Cuffe, O. J. Holland, A.V. Perkins, Mitochondrial dysfunction in placental trophoblast cells experiencing gestational diabetes mellitus, J. Physiol. 599 (4) (2021) 1291–1305.
[85] K.R. Kay, C. Smith, A.K. Wright, A. Serrano-Pozo, A.M. Pooler, R. Koffie, M. E. Bastin, T.H. Bak, S. Abrahams, K.J. Kopeikina, D. McGuone, M.P. Frosch, T. H. Gillingwater, B.T. Hyman, T.L. Spires-Jones, Studying synapses in human brain with array tomography and electron microscopy, Nat. Protoc. 8 (7) (2013) 1366–1380.
[86] A. Shapson-Coe, M. Januszewski, D.R. Berger, A. Pope, Y. Wu, T. Blakely, R. L. Schalek, P.H. Li, S. Wang, J. Maitin-Shepard, N. Karlupia, S. Dorkenwald, E. Sjostedt, L. Leavitt, D. Lee, J. Troidl, F. Collman, L. Bailey, A. Fitzmaurice, R. Kar, B. Field, H. Wu, J. Wagner-Carena, D. Aley, J. Lau, Z. Lin, D. Wei, H. Pfister, A. Peleg, V. Jain, J.W. Lichtman, A petavoxel fragment of human cerebral cortex reconstructed at nanoscale resolution, Science 384 (6696) (2024) eadk4858.
[87] Y. Cheng, N. Grigorieff, P.A. Penczek, T. Walz, A primer to single-particle cryo-electron microscopy, Cell 161 (3) (2015) 438–449.
[88] X. Yan, S. Li, W. Huang, H. Wang, T. Zhao, M. Huang, N. Zhou, Y. Shen, X. Li, MPicker: visualizing and picking membrane proteins for cryo-electron tomography, Nat. Commun. 16 (1) (2025) 472.
[89] T.B. Blum, A. Hahn, T. Meier, K.M. Davies, W. Kühlbrandt, Dimers of mitochondrial ATP synthase induce membrane curvature and self-assemble into rows, Proc. Natl. Acad. Sci. U. S. A. 116 (10) (2019) 4250–4255.
[90] E. Buzzard, M. McLaren, P. Bragoszewski, A. Brancaccio, H.C. Ford, B. Daum, P. Kuwabara, I. Collinson, V.A.M. Gold, The consequence of ATP synthase dimer angle on mitochondrial morphology studied by cryo-electron tomography, Biochem. J. 481 (3) (2024) 161–175.
[91] L.V. Bock, H. Grubmüller, Effects of cryo-EM cooling on structural ensembles, Nat. Commun. 13 (1) (2022) 1709.
[92] K. Kelley, A.M. Raczkowski, O. Klykov, P. Jaroenlak, D. Bobe, M. Kopylov, E. T. Eng, G. Bhabha, C.S. Potter, B. Carragher, A.J. Noble, Waffle Method: a general and flexible approach for improving throughput in FIB-milling, Nat. Commun. 13 (1) (2022) 1857.
[93] J. Zhang, G. Ji, X. Huang, W. Xu, F. Sun, An improved cryo-FIB method for fabrication of frozen hydrated lamella, J. Struct. Biol. 194 (2) (2016) 218–223.
[94] M. Strauss, G. Hofhaus, R.R. Schröder, W. Kühlbrandt, Dimer ribbons of ATP synthase shape the inner mitochondrial membrane, EMBO J. 27 (7) (2008) 1154–1160.
[95] R. Danev, H. Yanagisawa, M. Kikkawa, Cryo-Electron microscopy methodology: current aspects and future directions, Trends Biochem. Sci. 44 (10) (2019) 837–848.
[96] J.A.G. Briggs, Structural biology in situ—the potential of subtomogram averaging, Curr. Opin. Struct. Biol. 23 (2) (2013) 261–267.
[97] K.M. Davies, B. Daum, V.A. Gold, A.W. Mühleip, T. Brandt, T.B. Blum, D.J. Mills, W. Kühlbrandt, Visualization of ATP synthase dimers in mitochondria by electron cryo-tomography, J. Vis. Exp. 91 (2014) 51228.
[98] R.K. Flygaard, A. Mühleip, V. Tobiasson, A. Amunts, Type III ATP synthase is a symmetry-deviated dimer that induces membrane curvature through tetramerization, Nat. Commun. 11 (1) (2020) 5342.
[99] A. Mühleip, R. Kock Flygaard, J. Ovciarikova, A. Lacombe, P. Fernandes, L. Sheiner, A. Amunts, ATP synthase hexamer assemblies shape cristae of Toxoplasma mitochondria, Nat. Commun. 12 (1) (2021) 120.
[100] L. Dietrich, A.-N.A. Agip, C. Kunz, A. Schwarz, W. Kühlbrandt, In situ structure and rotary states of mitochondrial ATP synthase in whole *Polytomella* cells, Science 385 (6713) (2024) 1086–1090.
[101] A. Mühleip, R.K. Flygaard, R. Baradaran, O. Haapanen, T. Gruhl, V. Tobiasson, A. Maréchal, V. Sharma, A. Amunts, Structural basis of mitochondrial membrane bending by the I–II–III2–IV2 supercomplex, Nature 615 (7954) (2023) 934–938.
[102] W. Zheng, P. Chai, J. Zhu, K. Zhang, High-resolution in situ structures of mammalian respiratory supercomplexes, Nature 631 (8019) (2024) 232–239.
[103] J.R. Friedman, A. Mourier, J. Yamada, J.M. McCaffery, J. Nunnari, MICOS coordinates with respiratory complexes and lipids to establish mitochondrial inner membrane architecture, eLife 4 (2015).
[104] F. Waltz, R.D. Righetto, L. Lamm, T. Salinas-Giegé, R. Kelley, X. Zhang, M. Obr, S. Khavnekar, A. Kotecha, B.D. Engel, In-cell architecture of the mitochondrial respiratory chain, Science 387 (6740) (2025) 1296–1301.
[105] S.E. Siegmund, R. Grassucci, S.D. Carter, E. Barca, Z.J. Farino, M. Juanola-Falgarona, P. Zhang, K. Tanji, M. Hirano, E.A. Schon, J. Frank, Z. Freyberg, Three-Dimensional analysis of mitochondrial crista ultrastructure in a patient with leigh syndrome by In Situ Cryoelectron Tomography, iScience 6 (2018) 83–91.
[106] M.Y. Fry, P.P. Navarro, P. Hakim, V.Y. Ananda, X. Qin, J.C. Landoni, S. Rath, Z. Inde, C.M. Lugo, B.E. Luce, Y. Ge, J.L. McDonald, I. Ali, L.L. Ha, B. P. Kleinstiver, D.C. Chan, K.A. Sarosiek, L.H. Chao, In situ architecture of Opa1-dependent mitochondrial cristae remodeling, EMBO J. 43 (3) (2024) 391–413.
[107] K. Drożdżyk, M. Sawicka, M.-I. Bahamonde-Santos, Z. Jonas, D. Deneka, C. Albrecht, R. Dutzler, Cryo-EM structures and functional properties of CALHM channels of the human placenta, eLife 9 (2020) e55853.
[108] D. Bhella, Cryo-electron microscopy: an introduction to the technique, and considerations when working to establish a national facility, Biophysical Reviews 11 (4) (2019) 515–519.
[109] C.M. Zimanyi, M. Kopylov, C.S. Potter, B. Carragher, E.T. Eng, Broadening access to cryoEM through centralized facilities, Trends Biochem. Sci. 47 (2) (2022) 106–116.
[110] R.K. Hylton, M.T. Swulius, Challenges and triumphs in cryo-electron tomography, iScience 24 (9) (2021) 102959.
[111] R. Conrad, K. Narayan, Instance segmentation of mitochondria in electron microscopy images with a generalist deep learning model trained on a diverse dataset, Cell Syst. 14 (1) (2023) 58–71, e5.
[112] L. Lamm, S. Zufferey, H. Zhang, R.D. Righetto, F. Waltz, W. Wietrzynski, K. A. Yamauchi, A. Burt, Y. Liu, A. Martinez-Sanchez, S. Ziegler, F. Isensee, J. A. Schnabel, B.D. Engel, T. Peng, MemBrain v2: an end-to-end tool for the analysis of membranes in cryo-electron tomography, bioRxiv (2025), 2024.01.05.574336.
[113] M. Chen, J.M. Bell, X. Shi, S.Y. Sun, Z. Wang, S.J. Ludtke, A complete data processing workflow for cryo-ET and subtomogram averaging, Nat. Methods 16 (11) (2019) 1161–1168.
[114] T. Majtner, J.P. Kreysing, M.W. Tuijtel, S. Cruz-León, J. Liu, G. Hummer, M. Beck, B. Turoňová, cryoTIGER: deep-learning based tilt interpolation generator for enhanced reconstruction in cryo electron tomography, Commun. Biol. 8 (1) (2025) 1443.
[115] M. Harastani, G. Patra, C. Kervrann, M. Eltsov, Template Learning: deep learning with domain randomization for particle picking in cryo-electron tomography, Nat. Commun. 16 (1) (2025) 8833.
[116] S. Bhattacharjee, X. Feng, S. Maji, P. Dadhwal, Z. Zhang, Z.P. Brown, J. Frank, Time resolution in cryo-EM using a PDMS-based microfluidic chip assembly and its application to the study of HflX-mediated ribosome recycling, Cell 187 (3) (2024) 782–796.e23.